

Supplementary Information for “Mechanistic insights into nitrogen fixation by nitrogenase enzymes”

Joel B. Varley^{1,2}, Ying Wang¹, Karen Chan¹, Felix Studt³ and Jens K.
Nørskov^{1,3}

¹*Department of Chemical Engineering, Stanford University, Stanford, CA 94305-5025*

²*Lawrence Livermore National Laboratory, Livermore, CA 94550*

³*SUNCAT Center for Interface Science and Catalysis, Photon Science, SLAC National Accelerator
Laboratory, Menlo Park, CA 94025*

1 Computational Details

All reported calculations are based on density functional theory (DFT) using a real-space grid and projector-augmented wave (PAW) potentials as implemented in the GPAW code. [1, 2] The uniform grid-spacing was set to 0.18 Å for all calculations. Geometries were optimized using the GPAW code and the ASE simulation environment [3] with only the lowest energy adsorbate binding sites reported. Electron exchange and correlation terms were described with the use of the BEEF-vdW functional that combines generalized gradient exchange and correlation approximations with van der Waals correlation derived from the Langreth-Lundqvist non-local correlation functional [4, 5]. The BEEF-vdW functional was fitted specifically for applications in surface chemistry to accurately describe adsorbate-surface bonding, and details of the error estimation capabilities are described in Section 1.5. While BEEF-vdW was developed to most faithfully describe adsorbate-surface bonding and reaction energies, [4] we demonstrate in Sec. 1.6 that it also does a particularly good job of describing metal sulfide heats of formation relative to experimental values. This substantiates the results obtained for the FeMoco cluster which also includes open shell elements like Mo and Fe.

All integrations over the Brillouin zone were performed using only the Γ -point for the $20 \times 20 \times 20$ Å non-periodic supercells. The electronic structure calculations employed a Fermi-level smearing width, taken as 0.05 eV for the adsorbates, and 0.01 eV for all gas-phase calculations. All results were obtained with spin-polarized (spin-unrestricted) calculations and adopted the lowest energy adsorbate configurations bound to the model cluster described in Sec. 1.1. The vibrational modes of each adsorbate were calculated within the harmonic approximation and used to determine the zero-point energies, entropies, and heat capacities necessary to convert the DFT electronic energies to free energies and described in Sec. 1.2. The same process was performed for all gas phase molecules without any constraints of translational degrees of freedom and included in Sec. 1.3. Barriers for explicit proton transfers such as from the H_xS^* to NH_x^* species were calculated using the climbing nudged-elastic band (NEB) method [6].

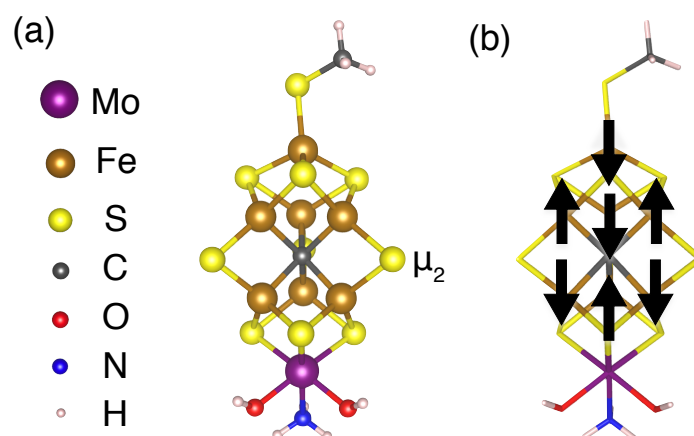


Figure S1: Schematic of the model cluster FeMoco cluster shown without protonated μ_2 S2B (a) and the lowest-energy antiferromagnetic coupling of the Fe assumed for the resting state (b).

All voltage-dependent electrochemical free energy pathways were constructed from the obtained free energies following the computational hydrogen electrode (CHE) model, [7] a framework described in Sec. 1.4. The determined theoretical overpotentials for each free energy pathway correspond to the maximum thermodynamic barrier for a given coupled proton and electron transfer and do not include kinetic barriers involved in the transfer. We considered an extensive list of possible intermediates and only include the lowest-energy pathways in the main manuscript.

In Section 2 we discuss additional details of the pathways presented in the main text, including the role of inhibitors and barriers for proton transfers from the S2B atoms. We supplement the results of the main text with additional calculations that assess the influence of charge and spin states with the use of the revised Perdew-Burke-Ernzerhof (RPBE) exchange-correlation functional [8, 9]. Results with RPBE yield the same qualitative conclusions but have slightly different energetics and are a valuable comparison, but they do not include the error estimation capabilities of BEEF-vdW.

1.1 The model cluster

All calculations are based on a model FeMoco cluster described previously, [9] where we adopt the most recent high-resolution crystallographic model of the cluster with C as the central interstitial atom. [10, 11] The resting state of the cluster adopted a $S = 3/2$ spin state and the lowest-energy antiferromagnetic magnetic ordering included in Fig. S1 that has been corroborated by experiment and previous calculations. [9, 12–20] While the crystal structure of the cluster is also now fairly well established, [10, 11, 21] several other aspects such as the charge, oxidation, and protonation states of the cluster remain largely unknown both for the resting state and during turnover conditions. For example, reports for the oxidation state have typically assumed Mo adopts a diamagnetic Mo^{IV} state and the Fe adopt a combination of Fe^{II} and Fe^{III} that are compatible with the observed $S = 3/2$ resting state (i.e. $2\text{Fe}^{\text{II}}-5\text{Fe}^{\text{III}}$, $4\text{Fe}^{\text{II}}-3\text{Fe}^{\text{III}}$, $6\text{Fe}^{\text{II}}-1\text{Fe}^{\text{III}}$, or 7Fe^{III}) [13, 19, 22] Recent experimental and theoretical observations dispute these claims and identify a Mo^{III} may be more likely in the FeMoco, with the strong possibility of mixed valency delocalization over Fe pairs ($\text{Fe}^{2.5}-\text{Fe}^{2.5}$) as seen in cubane analogs. [20] Even the charge of the resting state of the cofactor is not unambiguously known, with assigned values of 0 from DFT-based studies on the N-centered FeMoco to -3 based on assumptions coming

from studies on extracted and oxidized cofactors. [19, 23] To our knowledge the protonation state has only been addressed theoretically, [9, 16, 19, 24, 25] where it has been predicted that H atoms should favorably bind to the cluster under the potential regimes expected under turnover conditions within the enzyme.

Due to all of these uncertainties, we consider a range of both the formal charge of the cluster as well as the additional influence of the protonation state of the μ_2 S2B atoms to analyze the sensitivity of our conclusions. The model clusters presented in the main text assume a resting state that is uncharged and protonated on two μ_2 S based on the favorable energetics [9] but we consider multiple charge and protonation states and summarize the results in Sec. 2.1. For all intermediates we consider a number of configurations over the magnetic and spin degrees of freedom and all pathways reflect the lowest energy states. While we do find some quantitative changes depending on the combination of charge and protonation state, our qualitative conclusions remain unchanged. Namely, a reactive Fe edge site must first be exposed via the displacement of the μ_2 S2B to reduce N_2 under physiological conditions.

1.2 Adsorbate free energies

Adsorbate free energies were calculated by treating all of the adsorbate's $3N$ degrees of freedom as vibrational and neglecting changes in the nitrogenase vibrational modes due to the presence of adsorbates. [9, 26] The vibrational modes of each adsorbate were calculated within the harmonic oscillator approximation and used to determine the zero-point energies, entropies, and heat capacities necessary to convert the DFT electronic energies to Gibbs free energies [3, 9, 26, 27]. These contributions to the free energy ($G - E_{\text{elec}}$) are calculated from the optimized geometries and summarized in Table S1 at a temperature of 25°C.

Our model cofactor did not explicitly include a surrounding ligand network that can additionally stabilize intermediates via hydrogen bonding. To approximately account for these solvation effects in the vicinity of the cluster, we include additional corrections as detailed by Peterson *et al.* and adopted in previous studies [9, 26, 27]. A correction of 0.5 eV was justified for hydroxyl adsorbates bound directly to the surface (OH*), 0.25 eV when indirectly bound through other atoms (R-OH*), and 0.1 eV for bound CO* and CHO*. [26, 28, 29] We extend these corrections to “hydroxyl-like” NH* adsorbates that are directly bound (NH*, NH₂*, and NH₃*) and indirectly bound R-NH* species (N₂H*, N₂H₂*, N₂H₃*, N₂H₄*) and do not apply any solvation corrections to unhydrogenated N-containing species (N₂* and N*). We do not apply analogous corrections to the protonated or unprotonated S2B species. We note that these corrections do not influence the qualitative conclusions detailed in the main text.

1.3 Gas-phase species

The chemical potentials of gas-phase species were obtained by standard ideal gas methods by using the calculated electronic energy and vibrational modes. To obtain free energies for the energy pathway diagrams, the temperature was also taken as 25°C and pressure contributions were taken as described in the main text and in Table S2. This choice for the fugacity of nearly all gas-phase species does not lead to any qualitative differences in the observed pathways and intermediates. We also include additional corrections to the H₂ gas molecule as identified in a sensitivity analysis of the BEEF-vdW functional [30], which improves gas-phase energetics and leads to an additional stabilization of 0.04 eV per hydrogen atom.

Table S1: Contributions to the adsorbate free energy from the zero-point energy correction, enthalpic temperature correction, entropy, and the total free energy correction, respectively. All values are given in eV.

Adsorbate	ZPE (eV)	$\int C_P dT$ (eV)	$-TS$ (eV)	$G - E_{\text{elec}}$ (eV)
H*	0.18	0.01	-0.01	0.18
H-H*	0.36	0.01	-0.01	0.36
S*	0.04	0.04	-0.08	0.01
SH*	0.26	0.06	-0.11	0.21
SH-H*	0.44	0.07	-0.12	0.39
SH-H-H*	0.62	0.07	-0.13	0.57
H ₂ S*	0.51	0.06	-0.11	0.46
H ₂ S-H*	0.69	0.07	-0.12	0.64
H ₂ S-H-H*	0.87	0.07	-0.13	0.82
N ₂ *	0.20	0.05	-0.08	0.16
N ₂ -H*	0.38	0.06	-0.09	0.34
N ₂ -H-H*	0.56	0.06	-0.10	0.52
N ₂ H*	0.52	0.06	-0.09	0.48
N ₂ H-H*	0.70	0.06	-0.10	0.66
N ₂ H ₂ *	0.83	0.07	-0.12	0.79
N ₂ H ₃ *	1.15	0.08	-0.14	1.09
N ₂ H ₄ *	1.51	0.10	-0.18	1.43
N*	0.08	0.03	-0.05	0.06
NH*	0.38	0.03	-0.05	0.37
NH ₂ *	0.73	0.04	-0.05	0.72
NH ₃ *	1.06	0.06	-0.10	1.01
NH-SH*	0.64	0.09	-0.16	0.57
NH ₂ -S*	0.78	0.08	-0.13	0.72
NH ₂ -SH*	0.99	0.10	-0.17	0.92
CO*	0.22	0.06	-0.10	0.18
CHO*	0.50	0.07	-0.13	0.44
COH*	0.52	0.06	-0.10	0.48

Table S2: Assumed fugacity for each non-adsorbed gas-phase species, along with the calculated zero-point energy correction, enthalpic temperature correction, entropy contribution, and chemical potential. H₂ is the value used for the gas-phase hydrogen, while H₂ at a pressure of 101325 Pa (1 atm) is used for the computational hydrogen electrode (CHE).

Species	Fugacity (Pa)	ZPE (eV)	$\int C_P dT$ (eV)	$-TS$ (eV)	μ (eV)
H ₂	1013	0.27	0.09	-0.52	-0.16
H ₂ (CHE)	101325	0.27	0.09	-0.40	-0.04
N ₂	81060	0.15	0.09	-0.62	-0.38
NH ₃	1013	0.91	0.10	-0.71	0.30
H ₂ S	44076	0.40	0.10	-0.66	-0.15
CO	10132	0.13	0.09	-0.67	-0.45

Table S3: Energies and standard deviations obtained with BEEF-vdW. All energies in the ΔG column are relative to a vacant S2B site and referenced to the energies of H_2 , H_2S , N_2 , and CO gas phase molecules as summarized in Table S2, while those summarized in the ΔG^U column are referenced to the most favorable state prior to each proton-electron transfer and evaluated at a potential of 0 V vs RHE. The primes (') represent alternate higher-energy branches to the pathway for a given proton-electron step, and the superscript k represents the proton-shuffling steps which do not depend on the potential and are described in Sec. 2.3. Note minor differences in free energies for seemingly identical states correspond to differences in the chemical potential of the proton and electron pairs in the CHE compared to the pressure chosen for the $\text{H}_2(\text{g})$ reference (see Equations 4 and 5).

$\text{H}^+ + e^-$			
transfer index	Species	ΔG (eV)	ΔG^U (eV)
0	S^*	-1.96 ± 0.32	–
1	SH^*	-1.72 ± 0.10	0.17 ± 0.28
2	SH-H^*	-0.83 ± 0.14	0.82 ± 0.09
2'	H_2S^*	-0.25 ± 0.14	1.40 ± 0.09
3	H^*	-0.39 ± 0.08	0.39 ± 0.10
3'	$\text{H}_2\text{S}^*-\text{H}^*$	-0.20 ± 0.18	0.57 ± 0.15
4	*	–	0.34 ± 0.36
4'	H^*-H^*	-0.01 ± 0.19	0.33 ± 0.18
	N_2^*	0.18 ± 0.12	–
	N_2^-*	-0.02 ± 0.11	–
5	N_2H^*	0.38 ± 0.38	0.34 ± 0.38
5'	$\text{N}_2\text{H}^*-\text{SH}^*$	0.25 ± 0.42	1.92 ± 0.38
5''	$\text{N}_2\text{H}^*-\text{S}^*$	0.31 ± 0.55	2.22 ± 0.27
6	N_2H_2^*	0.34 ± 0.45	-0.10 ± 0.08
7	N^*	0.30 ± 0.51	-0.20 ± 0.10
7 ^{k,a}	NH^*-SH^*	-0.47 ± 0.39	-0.77 ± 0.22
7 ^{k,b}	NH_2^*-S^*	-1.39 ± 0.40	-0.92 ± 0.04
8	S^*	-0.21 ± 0.14	-0.73 ± 0.16
8'	NH^*	-0.90 ± 0.36	-1.26 ± 0.20
9'	NH_2^*	-1.59 ± 0.13	-0.76 ± 0.33
10'	NH_3^*	-0.88 ± 0.13	0.65 ± 0.09
	CO^*	-1.19 ± 0.41	–
1'	COH^*	-0.35 ± 0.41	0.79 ± 0.05
1''	CHO^*	-0.67 ± 0.33	0.46 ± 0.11

1.4 The computational hydrogen electrode

The CHE provides a framework for describing the free energy change of a reaction step that involves an electrochemical transfer of a proton-electron pair as a function of the applied potential. This approach has successfully described qualitative and quantitative trends in a variety of important electrochemical reactions without having to explicitly simulate solvated protons [7,26,31–33]. In the CHE model, zero voltage is defined based on the reversible hydrogen electrode (RHE), in which the reaction



is defined to be in equilibrium at zero voltage, at all values of pH, at all temperatures, and with H_2 at a pressure of 101325 Pa (1 atm). This establishes that the chemical potential of a proton-electron pair is equal to half of the chemical potential of the H_2 molecule at a potential of 0 V. The chemical potential of the proton-electron pair is adjusted as a function of the electrochemical potential by the relationship $\Delta G = -eU$, where e is the elementary positive charge and U is the applied bias potential. By combining these relationships the chemical potential of a proton-electron pair can be expressed as a function of the applied potential U by

$$\mu[\text{H}^+ + e^-](U, T) = \frac{1}{2}\mu[\text{H}_2](T, p = 1 \text{ atm}) - eU, \quad (2)$$

where T is the temperature and U is defined relative to the RHE potential. The reaction step involving a proton-electron transfer that exhibits the largest barrier at a potential of 0 V vs RHE is identified as the potential-limiting step, and the potential necessary to reduce the free energy change of this step to zero corresponds to the theoretical overpotential. In the main text we limit our analyses to overpotentials of -0.7 V vs RHE as an approximate upper-bound to what could be achieved with the hydrolysis of two MgATP per proton-electron transfer within the enzyme (0.67 eV) [12, 34, 35]. This same constraint was considered in other works in the form an explicitly chosen value for the chemical potential of the H_2 reference energy [15, 16, 36].

We note that pH effects do not influence the reported potentials relative to the RHE redox potential by definition. However, relative to other redox potentials the influence of pH can be described via Nernst's equation. For the example of a potential V measured relative to a redox potential V_0 defined at 0 pH like the standard hydrogen electrode (SHE), the potential would be determined by

$$V(\text{pH}) = V_0 - 0.0591 \text{ pH}. \quad (3)$$

1.5 Ensemble error analysis

To assess the uncertainty in the calculated DFT total energies, we employ the error estimation capabilities in the BEEF-vdW functional as described extensively in Refs. 4 and 37. In this procedure an ensemble of density functionals are generated around BEEF-vdW that randomly sample a probability distribution for model parameters for the exchange and correlation. By construction, the distribution of model parameters is designed to reproduce known energetic errors that have been mapped to uncertainties in the exchange and correlation parameterization [4]. For each adsorbate and molecule considered in this work, we randomly sampled an ensemble of 2000 functionals to generate a distribution of total energies, assuming the relaxed geometry as obtained with BEEF-vdW. As in Ref. 37, we use the standard deviation of the obtained ensemble of energies to estimate the error bar in the DFT total energy.

The ensemble from Ref. 4 was originally designed to reproduce the mean errors on several properties such as molecular reaction energies, reaction barriers, adsorption energies, and even solid-state cohesive energies and lattice constants. As the current work is concerned with surface chemistry, we adopt the procedure of Ref. 37 to rescale the fluctuations in the ensemble of functionals to reproduce the mean error of only the ensemble of benchmark adsorption data. This involves rescaling the obtained distribution of ensemble energies by 0.683 [4,37]. We summarize the obtained free energies and their standard deviations in Table S3. Considering we can reference the free energies directly to a single common state (i.e. an unprotonated S2B in the case of the main text, or the vacant S2B site in Table S3) and an initial state prior to a proton-electron transfer, we can identify two uncertainties. The former (ΔG) represents the uncertainty in the free energy of a given state on an absolute scale defined by the reference state(s), while the latter (ΔG^U) represents the uncertainty in the theoretical overpotential predicted for a given proton-electron transfer step. The energies in Table S3 are defined relative to the free energies of the cofactor with a μ_2 S2B removed (*) and H_2 , H_2S , N_2 , and CO gas phase molecules. For the example of the SH-H* intermediate, the energy would be defined as

$$\Delta G[\text{SH-H}^*] = G[\text{SH-H}^*] - G[*] - G[\text{H}_2\text{S}(\text{g})], \quad (4)$$

which yields a ΔG of -0.83 eV with a standard deviation of 0.14 eV as included in Table S3. The corresponding example for the uncertainty in the limiting potential of this step would

$$\Delta G^U[\text{SH-H}^*] = G[\text{SH-H}^*] - G[\text{SH}^*] - G[\text{H}^+ + e^-], \quad (5)$$

which has a ΔG^U of 0.82 eV \pm 0.09 eV as summarized in Table S3 and discussed in the main text.

1.6 BEEF-vdW description of metal sulfides

To assess the reliability of the BEEF-vdW functional in describing the chemistry of the FeMoco cluster, we computed the heats of formation for a number of different metal sulfide compounds, i.e. the solid state analogs to the cluster, and compared the results to their experimental values in Fig. S2. In this figure we define the theoretical formation enthalpy of a transition metal sulfide M_xS_y by

$$\Delta H^{\text{theory}} = E_{M_xS_y} - xE_M - y(E_{\text{H}_2\text{S}} - E_{\text{H}_2}), \quad (6)$$

where we reference the sulfur reservoir to H_2S and H_2 using their zero-point energy corrected electronic energies, $E_{\text{H}_2\text{S}}$ and E_{H_2} . Experimental sulfide formation enthalpies were obtained from References 38, 39, and 40 and converted from an elemental sulfur reference to a consistent H_2S reference via

$$\Delta H^{\text{expt}} = \Delta H^{\text{expt}}(\text{sulfur ref.}) + y\Delta H^{\text{expt}}(\text{H}_2\text{S}), \quad (7)$$

where the experimental H_2S formation enthalpy $\Delta H^{\text{expt}}(\text{H}_2\text{S})$ is -0.182 eV [38].

These results were performed independently from the results of the main text and only serve to illustrate the BEEF-vdW functional accurately describes the energetics associated with the transition metal-sulfur bonds that are perturbed and even broken throughout the N_2 reduction reaction. Specifically, the calculations were performed using spin-polarized, plane-wave DFT with ultrasoft pseudopotentials as implemented in the Quantum ESPRESSO software package [41]. The plane wave and density cutoffs for all systems that did not include Fe were 500 and 5000 eV for systems, while higher plane wave and density cutoffs of 800 and 8000 eV were included for Fe and the Fe sulfides. The Brillouin zone was sampled using Monkhorst-Pack k -point grids of $(\sim 30/a, \sim 30/b, \sim 30/c)$, where a , b , and c are the unit cell dimensions.

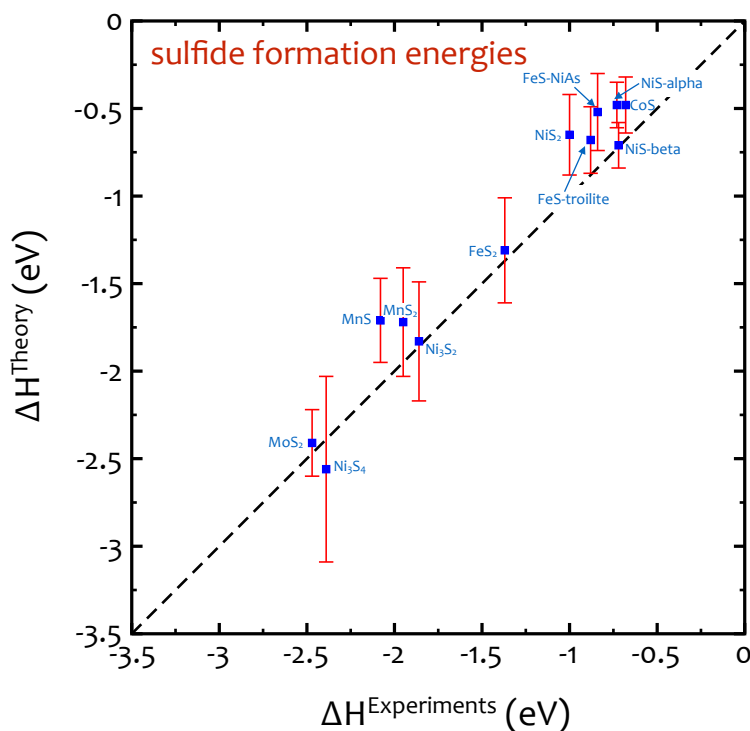


Figure S2: Comparison of experimental and theoretical formation enthalpies for a number of metal sulfides as obtained with the BEEF-vdW functional [38–40]. The results include the error estimation of BEEF-vdW and indicate good agreement with experimental values well within the error of the calculations.

The error estimated from the BEEF-vdW ensembles follow the same procedure as in Sec. 1.5. Even accounting for the uncertainty in the calculated enthalpies, the results included in Fig. S2 indicate good agreement between theory and experiment and give confidence in the description provided by the BEEF-vdW functional for the FeMoco cluster.

2 Additional details of intermediates and reduction pathways

2.1 Binding and charge states of the cofactors

Another heavily investigated aspect of the FeMoco is the formal charge state of the active site during different stages of substrate reduction. There has been a strong correlation between charge and catalytic activity in studies of the full enzyme system, [13, 16, 19, 42, 43] as well as its role in substrate binding in isolated cofactors. [44] Therefore we consider a range of both the formal charge of the cluster as well as the additional influence of the protonation state of the μ_2 S atoms to analyze the sensitivity of our conclusions. We include results in Table S4 for initial uncharged $S = 3/2$ reference states with 0 ($n = 0$) or 2 ($n = 2$) protons on the μ_2 S2B and the antiferromagnetic coupling shown in Fig. S1.

Table S4 highlights how the relative free energies associated with vacating the S2B site and subsequently binding N_2 -related species are generally insensitive to the cluster charge and protonation state. Specifically, we find that the predicted free energies necessary to protonate

Table S4: Theoretical overpotentials calculated for each specified proton-electron transfer with respect to the step in parenthesis. The binding energies of N_2^* and NH_3^* are also included relative to a vacant μ_2 S2B site (*). The free energies do not include any additional stabilization effects discussed in Sec. 1.2.

Adsorbate	$n = 2$				$n = 0$			
	+1	0	-1	-2	+1	0	-1	-2
SH* (S*)	-0.04	0.23	0.46	0.76	0.10	0.08	0.21	0.33
SH*-H* (SH*)	1.05	0.81	0.65	0.68	0.83	0.83	0.63	0.58
H ₂ S* (SH*)	1.09	1.43	1.70	1.64	0.93	1.21	1.46	1.74
* (SH*)	1.56	1.55	1.58	1.80	1.51	1.52	1.53	1.67
H* (SH*-H*)	0.11	0.27	0.54	0.44	0.30	0.26	0.42	0.66
H*-H* (H*)	0.47	0.29	0.55	0.43	0.20	0.41	0.29	0.54
* (H*)	0.28	0.36	0.27	0.57	0.26	0.31	0.36	0.32
N ₂ H* (*S)	2.86	3.02	3.09	3.26	2.92	3.00	2.93	3.01
N ₂ H* (* or N ₂ *)	0.68	0.59	0.66	0.48	0.69	0.67	0.66	0.69
NH ₃ * (NH ₂ *)	0.59	0.73	1.03	1.21	0.37	0.70	0.85	0.91
N ₂ * (*)	0.13	0.25	0.07	-0.37	-0.08	0.01	0.22	0.06
NH ₃ * (*)	-0.41	-0.17	0.06	0.29	-0.56	-0.15	0.10	0.32

and displace the μ_2 S2B remain lower than that required to initiate the reduction of N_2 on the intact cluster. This is readily seen by comparing the free energies for N_2H^* formation with (*S) and without the S (*) present, as well as comparing the relative energies of the steps prior to displacing the S2B as an H_2S species. Our pathways indicate that the formation of a hydride ($\text{SH}^*\text{-H}^*$) is more favorable than forming a bound or dissociated H_2S species, independent of the charge state. After the hydride formation, the free energy required to additionally protonate and dissociate the S2B as H_2S (leaving an H^* intermediate) is reduced to within the biologically achievable potentials for all considered charge states. Furthermore, the free energy of the N_2H^* on the μ_2 site with the S2B removed is consistently drastically lower than when it is present.

We find that for the protonated cluster, the binding energy of N_2 generally becomes more favorable for more negatively-charged clusters for our model system. When calculated with BEEF-vdW, we find that the N_2 binding becomes favorable even for a singly-charged cluster, with the calculated binding energy of -0.02 ± 0.11 eV. In contrast, CO strongly binds with little sensitivity to the cluster charge state. In the main text we also include the change in charge density upon charging of the cluster for the N_2^* in the -1 and neutral charge states. The charge density isosurface indicates that the favorably bound N_2^* becomes slightly polarized upon binding to the negatively-charged cluster. The accumulation of charge at the end of the N_2^* would expectedly increase the likelihood for a proton transfer that would initiate the N_2 reduction at biologically compatible overpotentials as discussed in the main text. While our results suggest a relatively minor influence of the cluster charge and S2B protonation state on the overall energetics for displacing a μ_2 S2B to initiate N_2 reduction, these results may indicate the cluster charge state could play a role in the overall kinetics.

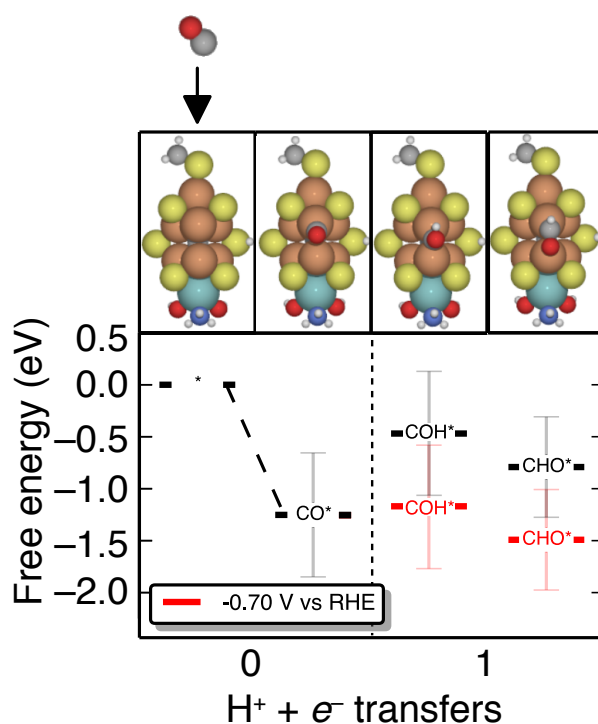


Figure S3: Free energy diagram for the adsorption of CO on the vacant μ_2 S2B site and the first proton-electron transfer to initiate CO reduction as calculated with BEEF-vdW. The black pathways are shown at 0 V vs RHE while the red pathways are shown at a potential of -0.7 V vs RHE as described in the main text. The error bars represent the standard deviation of the ensemble of BEEF-vdW energies relative to the free energy of the vacant μ_2 site (*).

Table S5: Representative magnetic and electronic spin states for relevant intermediates. Values correspond to the protonated cluster in the -2 charge state assuming the μ_2 site associated with the Fe4 and Fe5 sites.

Adsorbate	Fe1	Fe2	Fe3	Fe4	Fe5	Fe6	Fe7	Spin
S*	-3.2	2.8	2.8	-3.0	2.7	-2.5	-2.5	3/2
SH*	-3.3	2.8	2.8	-3.0	2.1	-2.6	-2.5	2
SH-H*	-3.3	2.8	2.8	-3.0	1.5	-1.4	-2.5	3/2
H*	-3.2	2.9	2.9	-2.8	3.0	-2.5	-2.4	1
*	-3.0	2.4	2.4	-2.9	2.7	-2.4	-2.3	3/2
H-H*	-3.2	2.8	2.7	-3.1	0.7	-2.5	-2.5	5/2
N ₂ *	-2.5	2.3	2.3	-1.6	2.4	-2.0	-2.0	1/2
N ₂ H*	-3.2	2.8	2.8	-1.7	2.3	-2.6	-2.5	1
N ₂ H ₂ *	-3.2	2.9	2.9	-2.5	2.0	-2.6	-2.6	3/2
N*	-3.1	2.8	2.8	-2.2	2.1	-2.5	-2.4	1
NH-SH*	-3.4	3.0	2.9	-1.6	1.9	-2.7	-2.6	1
NH ₂ -S*	-3.5	3.0	3.0	-1.3	1.8	-2.6	-2.7	1
NH ₃ *	-2.9	2.3	2.3	-2.8	2.6	-2.3	-2.2	3/2

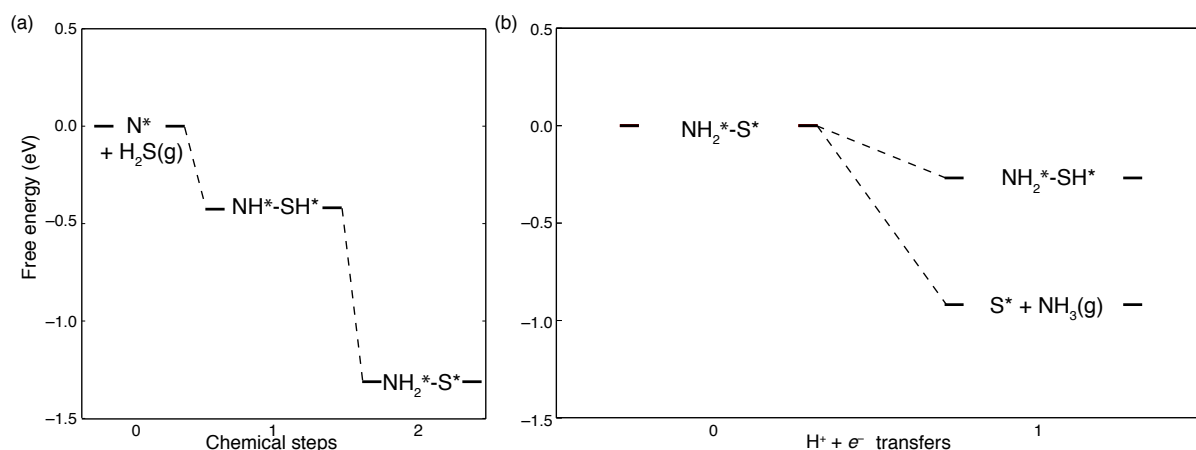


Figure S4: Free energy diagram for (a) the reabsorption of the protonated S2B onto the cluster (not including the kinetic barriers) and (b) the final proton-electron transfer of the N_2 reduction pathway after the S2B has reabsorbed and formed a $NH_2^*-S^*$ intermediate as calculated with RPBE. All pathways are shown at 0 V vs RHE, where it is already thermodynamically preferable to transfer protons from the S2B to bound N^* species in (a) or to protonate the NH_2^* and form NH_3 rather than reprotonating the S2B in (b). The free energy of initial reference state of the N^* in (a) and the $NH_2^*-S^*$ in (b) is set to 0 in each figure for illustrative purposes.

2.2 Inhibition of N_2 reduction by CO

Assessing the free energies summarized in Table S3, we find the binding energy of the CO^* is much stronger than other relevant intermediates such as H^* , H_2S^* , N_2^* , and NH_3^* within the uncertainty of the calculations. This is consistent with the binding of CO at a vacant μ_2 site as revealed by the high-resolution X-ray diffraction measurements of the CO-inhibited FeMoco [21]. In addition, reduction of CO^* also requires a larger electrochemical potential compared to N_2 when following the analogous distal protonation pathway to COH^* , as illustrated in the free energy diagram in Fig. S3. Note that H_2 can be easily evolved from the other μ_2 S2B sites at low electrochemical potentials even while the CO^* blocks the μ_2 Fe edge sites from participating in other substrate reduction [9] and can thus account for why only H_2 evolution is observed for CO-inhibited samples [45]. Overall our predicted theoretical overpotentials required for the reduction of CO^* are still within the bounds accessible within the enzyme, but the yield of CO-derived products is known to be far lower than that of N_2 [46, 47]. From our calculations we cannot provide an explanation for the disparity in CO vs N_2 reduction rates, but acknowledge that kinetics, mass and electron transport, and details of the ligand environment all likely contribute. A tendency to block the highly reactive μ_2 site is likely a general trend for other inhibitors of N_2 reduction, as μ_2 active site can be easily blocked by alternate adsorbates that are too strongly bound to be dissociated or too difficult to reduce under the physiological electrochemical conditions within the enzyme.

2.3 Identifying kinetic barriers

Following our predicted full free energy pathway for N_2 reduction, there are two steps that must involve a transfer of adsorbed protons on the S2B to the N_2 -derived intermediates to be compatible with experimental observations of 8-proton/electron transfers associated with the reduction reaction [12]. To identify and quantify possible barriers for this proton transfer to the NH_x^* species from the protonated S2B, we performed NEB calculations using the RPBE functional.

We calculate a barrier of 0.60 eV for the first transfer from the doubly-protonated S2B (H_2S) to an adsorbed N^* species to form the thermodynamically-favored $\text{NH}^*\text{-SH}^*$ intermediate (see Fig. S4a and Table S3). For the second proton transfer we calculate a barrier of 0.45 eV to form the thermodynamically favored $\text{NH}_2^*\text{-S}^*$ intermediate. A subsequent proton-electron transfer to the NH_2^* to form the second NH_3 is thermodynamically preferred over reprotonating the S2B, as seen in Fig. S4b. We emphasize that these barriers are only approximate estimates for barriers in the real enzyme system and expect the ligand environment has a significant effect in making the kinetics even more favorable under typical turnover conditions. This will have to be validated in subsequent theoretical studies that treat the ligand environment explicitly or experimentally via ligand engineering.

2.4 Optimized geometries

Representative optimized geometries of each adsorbate reported in the manuscript are given in the xyz file format with Cartesian coordinates (with atomic positions in Å) below.

S*

33

C	11.58210591	11.89122487	8.84550254
C	15.49248525	13.30604425	3.83515935
H	7.77113177	12.76974337	12.87238728
H	7.66296463	11.25471699	13.51704883
H	6.55915916	11.75512048	12.39586507
H	14.71560903	14.03321173	3.60258774
H	16.39601452	13.56030532	3.28114627
H	15.16333019	12.30854944	3.54809562
H	9.31138922	8.61686058	12.28870614
H	9.77508095	9.86594688	6.13808683
H	6.75648745	9.88520563	9.64664862
H	14.00619294	9.87492731	11.09492843
Mo	8.75427312	10.75071300	10.99123379
O	6.90602797	10.42786721	10.43032289
O	8.84205808	9.44443987	12.44978866
N	7.53482177	11.80491871	12.67338837
S	11.96485963	14.93390926	10.02602159
S	14.74892484	12.69729689	8.82928847
S	12.38145525	13.93349006	6.40211588
S	13.36059138	10.53781303	6.38564384
S	8.58799320	12.91607432	9.73468413
S	10.80436312	11.75937280	12.03660690
S	13.29893151	9.26722504	10.11816440
S	9.64786430	9.29514480	9.40302992
S	9.53782770	11.18969658	6.24656102
S	15.92171955	13.38166305	5.61353404
Fe	12.70379487	13.53221768	8.56840925
Fe	11.63410785	11.89181273	6.87666231
Fe	9.68796892	11.38717237	8.55629450
Fe	11.33744672	10.52807413	10.26841932
Fe	13.33135680	11.00187399	8.60241143
Fe	14.15542854	12.59349305	6.66979187
Fe	10.79483565	13.10823032	10.21678749

SH*

34

C	11.56252467	11.95188837	8.88876507
C	15.52075077	13.36799108	3.82474744
H	7.69043669	12.76626153	12.88297996
H	7.64058038	11.25903953	13.54790316
H	6.50953805	11.70723243	12.43631996
H	14.72858813	14.10532129	3.70478303
H	16.39629455	13.69033793	3.26121205
H	15.18838980	12.40242974	3.44629260
H	10.96313286	15.78917395	9.25615715
H	9.31089278	8.62505402	12.30585892
H	9.78862391	9.86910282	6.16688823
H	6.80046974	9.82825789	9.65244642
H	14.00342155	9.92517379	11.13655724
O	6.91185841	10.37172793	10.44179299
O	8.84466001	9.45114552	12.48337084
N	7.48789851	11.79137258	12.69713614
S	11.81265587	15.15838207	10.09352688
S	14.74065956	12.71781262	8.88555363
S	12.36620566	13.93103629	6.38524523
S	13.34844417	10.50092776	6.42983239
S	8.51893368	12.90299852	9.73448173
S	10.75594211	11.83014970	12.09447904
S	13.26721323	9.32175726	10.17919614
S	9.68810132	9.31827564	9.46126971
S	9.55182360	11.19126840	6.27746345
S	16.02578593	13.25789411	5.58257571
Fe	12.67859118	13.59683377	8.60315032
Fe	11.64914583	11.91679235	6.89956678
Fe	9.68521860	11.40311894	8.58190083
Fe	11.33618878	10.60941499	10.33151390
Fe	13.33120060	11.05185145	8.64202628
Fe	14.20287908	12.56130065	6.64687662
Fe	10.69509293	13.13239315	10.25092503
Mo	8.73994078	10.75346206	11.02671244

SH-H*

35

C	11.56440177	11.70932318	8.75373126
C	15.64960529	13.39688542	3.98553209
H	8.21165143	13.01132090	12.85403673
H	7.79182286	11.50146067	13.39352782
H	6.84555338	12.26861877	12.28726262
H	14.93360279	14.19459200	3.79390846
H	16.56380409	13.59509784	3.42526324
H	15.23615941	12.44168261	3.66489362
H	10.24805978	15.25083967	8.68778474
H	9.41553076	9.03631882	12.69516278
H	9.70257125	10.20563811	5.74740488
H	6.56968198	10.33166702	9.76900719
H	14.00933611	9.78582907	11.06732048
H	12.32555986	13.14525861	10.43123521
Mo	8.82219296	10.82442356	10.92606442
O	6.88409009	10.42531895	10.67514366
O	8.61715810	9.49962606	12.41788073

N	7.80243142	12.12293884	12.58986904
S	11.11747099	14.96024091	9.68328297
S	14.64327417	12.80495713	8.96990709
S	12.38395226	14.07129233	6.60518522
S	13.43751462	10.66988124	6.29592812
S	8.55099982	12.77556313	9.57319790
S	10.90017331	11.48568696	11.95194877
S	13.39366887	9.15721258	10.04439160
S	9.55514808	9.21922452	9.34182561
S	9.54228945	11.50165739	6.08909327
S	16.11325778	13.34825491	5.75949762
Fe	12.55997007	13.41916364	8.74185672
Fe	11.70884888	11.92625843	6.80100965
Fe	9.69171723	11.24658168	8.39481391
Fe	11.36444564	10.28454734	10.13269646
Fe	13.39561584	10.95119125	8.55992840
Fe	14.21209556	12.79149940	6.75020242
Fe	10.70491017	12.76557017	10.15324149

*** (S2B removed)**

32

C	11.56830187	11.86456145	8.87193172
C	15.50726671	13.30808753	3.83324490
H	7.75894353	12.84010228	12.90076064
H	7.68931895	11.30402884	13.50497597
H	6.59791905	11.79167972	12.37158729
H	14.71825609	14.03026054	3.63071311
H	16.39366938	13.57663297	3.25859269
H	15.17972538	12.31184429	3.53908671
H	9.19847147	8.63892256	12.28091108
H	9.85437066	9.85101994	6.11063688
H	6.78508798	9.83706852	9.75661837
H	14.01314521	9.79093711	11.07593479
Mo	8.79922899	10.82941446	11.00301428
O	6.92612167	10.44688152	10.48905584
O	8.78834004	9.49249904	12.46065860
N	7.56388123	11.87297619	12.67286177
S	14.73011837	12.78306881	8.95176315
S	12.29788482	14.01967651	6.46440815
S	13.39532263	10.58995653	6.39306384
S	8.53930435	12.94053251	9.65710734
S	10.88481865	11.71305507	12.11870763
S	13.30769912	9.22268038	10.07478724
S	9.62948932	9.29955066	9.44350720
S	9.57551595	11.16535111	6.22397790
S	15.97980982	13.35992551	5.60222390
Fe	12.64109763	13.52370839	8.62506833
Fe	11.64538620	11.92810851	6.89084763
Fe	9.68512576	11.36670065	8.52514132
Fe	11.36972977	10.48686944	10.29113804
Fe	13.36120053	11.03846297	8.62905270
Fe	14.17840173	12.66331464	6.69980583
Fe	10.64771060	12.90957079	10.28561297

H*

33

C	11.60797285	12.04914363	8.90320422
C	15.44880494	13.20144265	3.72859773
H	7.81038341	12.77017337	12.99005666
H	7.61748755	11.22481861	13.53511284
H	6.57187698	11.84228174	12.42057623
H	14.63755943	13.90183673	3.52810832
H	16.31045090	13.46804815	3.11465663
H	15.13332821	12.18945006	3.48124971
H	9.34408355	8.67171604	12.27427659
H	9.79302761	10.07439257	6.14486377
H	6.79849866	9.95469584	9.65658941
H	14.01573999	9.98483662	11.13471954
Mo	8.77291681	10.82602379	11.02474465
O	6.93383300	10.48845326	10.44815093
O	8.87424916	9.49467734	12.45607664
N	7.54160242	11.83050968	12.72276973
S	14.81784074	12.81772451	8.86782923
S	12.43631006	14.10276853	6.44874545
S	13.32600275	10.62144361	6.42824809
S	8.57831011	13.00876717	9.80339107
S	10.80445687	11.85097287	12.10511987
S	13.30391253	9.39151496	10.15345438
S	9.69051136	9.42007242	9.41790059
S	9.55187606	11.39162414	6.29415666
S	15.98135260	13.31818167	5.47730782
Fe	12.74803417	13.71064800	8.65464933
Fe	11.66058480	12.07993339	6.92045054
Fe	9.72059973	11.52644735	8.60011481
Fe	11.36759033	10.66465947	10.30978122
Fe	13.36660335	11.15088573	8.64731367
Fe	14.21917156	12.65303032	6.64766526
Fe	10.77135502	13.19689646	10.29529378
H	11.80330960	14.50001766	9.93827247

H-H*

34

C	11.49604442	11.88292974	8.87848695
C	15.40901564	13.20977665	3.86907932
H	7.71487951	12.61384786	13.01110522
H	7.54195920	11.05053961	13.50595591
H	6.49981860	11.68390504	12.39634844
H	14.59105040	13.86809682	3.57529070
H	16.28403084	13.43205376	3.25765417
H	15.11989000	12.17117062	3.72118537
H	9.30202433	8.55088810	12.18464215
H	9.78092243	10.14936183	6.04349626
H	6.76461975	9.86502558	9.61889316
H	13.97553491	10.02182300	11.16975838
Mo	8.72495181	10.74480583	11.00187080
O	6.88920809	10.39909673	10.41243755
O	8.83756052	9.37009814	12.39258332
N	7.46527054	11.67941141	12.71164826
S	14.67465487	12.98138335	9.01759622
S	12.30424140	14.22704152	6.60181472

S	13.40668654	10.83108955	6.44168525
S	8.52407121	12.94838737	9.79920089
S	10.74775744	11.78368692	12.08543930
S	13.34867543	9.41783430	10.13901662
S	9.64860781	9.34060382	9.37090998
S	9.51542719	11.45690460	6.24492872
S	15.88782880	13.50800382	5.61047355
Fe	12.53190303	13.70441820	8.79569700
Fe	11.62239547	12.10109566	6.95768963
Fe	9.62303375	11.44302375	8.57147935
Fe	11.30889502	10.55470292	10.30139437
Fe	13.31191669	11.20930725	8.67471044
Fe	14.14287923	12.93292174	6.84393093
Fe	10.73636157	13.12004270	10.25516900
H	11.10235978	14.48044127	9.22461552
H	12.31714335	13.85358786	10.45184240

H₂S*

35

C	11.55636651	11.83307432	8.82420267
C	15.49987334	13.29297614	3.99481485
H	8.22617487	12.88383452	12.95123454
H	7.81648536	11.35082587	13.42797937
H	6.89747239	12.13293715	12.31036368
H	14.70679663	14.02211184	3.83063148
H	16.36552227	13.56168662	3.38910724
H	15.15239075	12.30189143	3.70398934
H	10.68596987	15.49679687	9.47389138
H	9.42438234	8.99237196	12.77402610
H	9.83599375	10.08637369	5.83036817
H	6.81238765	9.46878912	11.08415002
H	14.30636352	9.18690352	10.89116322
H	13.41593863	8.03519410	9.54781082
Mo	8.91664119	10.75811914	10.95295237
O	7.00369589	10.29260863	10.61163065
O	8.61920372	9.33262322	12.36826232
N	7.84615124	11.99563058	12.64453257
S	11.61476390	14.83789831	10.20300797
S	14.59733985	12.72395731	9.02180554
S	12.44073606	14.07296807	6.60800155
S	13.43528950	10.67184755	6.38490253
S	8.52539078	12.72146713	9.59689821
S	10.97389308	11.40251669	12.05745732
S	13.38092881	9.35292610	9.90237213
S	9.75984732	9.19513807	9.34960552
S	9.59807013	11.38490004	6.10982144
S	16.03386184	13.30482053	5.74862274
Fe	12.57116705	13.43804988	8.71419283
Fe	11.70585122	11.98207436	6.85395558
Fe	9.68880845	11.22165537	8.42360391
Fe	11.44548741	10.39157067	10.14971914
Fe	13.29378753	11.04454093	8.55591677
Fe	14.20731204	12.73148887	6.83720873
Fe	10.63135217	12.74973715	10.32227201

H₂S-H*

36

C	11.51464000	11.80262926	8.66776435
C	15.41267729	13.32405771	3.51420944
H	8.08341369	13.00440663	12.69807013
H	7.65215482	11.46726659	13.18966853
H	6.73262634	12.25896468	12.06010308
H	14.62321149	14.07058889	3.35644756
H	16.27507534	13.57099301	2.88013478
H	15.04277126	12.32634023	3.24771399
H	10.82109105	15.51944856	9.42980755
H	8.99813136	8.71017184	12.05249342
H	9.88782285	10.15510214	5.52271227
H	6.75655836	9.88301468	9.51882275
H	13.11999336	9.02402421	12.33670269
Mo	8.76618025	10.80258633	10.73913804
O	6.81676047	10.39986500	10.35025524
O	8.32817716	9.40138414	12.20829005
N	7.68732441	12.11252819	12.39577093
S	11.66002795	14.81632835	10.23378675
S	14.82709763	12.82038435	8.67580514
S	12.43595603	14.12596241	6.30748350
S	13.44728142	10.69700421	6.12142726
S	8.48136331	12.72705670	9.28459461
S	10.77625943	11.45303046	11.95311589
S	12.13888790	8.34710224	11.69407512
S	9.62199436	9.18250050	9.18490846
S	9.61194452	11.43993339	5.87003738
S	15.99657997	13.35627244	5.25751362
Fe	12.64920921	13.54463157	8.50917296
Fe	11.69765242	12.01506980	6.72637595
Fe	9.68216234	11.18738351	8.18370802
Fe	11.41133350	10.30253020	10.06798922
Fe	13.36208229	11.10092934	8.35634026
Fe	14.25437605	12.78875900	6.49729480
Fe	10.55832788	12.72942767	10.12495381
H	13.10736920	9.92090539	9.51431333
H	13.03719243	7.61320404	10.98975455

H₂S-H-H*

37

C	11.46082161	11.95077927	8.63116936
C	15.40050663	13.23984945	3.64919373
H	8.02835536	12.85864257	12.68925092
H	7.69780478	11.31384060	13.17308488
H	6.75167867	12.03159851	12.03258948
H	14.62844929	14.00423221	3.57141768
H	16.22541129	13.48807175	2.98100426
H	14.98947854	12.27091878	3.37012745
H	10.77427960	15.60858468	9.29953182
H	9.13097523	8.52648298	11.92922001
H	9.97984496	10.09511651	5.57495161
H	6.68052368	10.16153809	9.59213203
H	13.08253143	9.02774761	12.26959902
Mo	8.90553648	10.75144845	10.75012467
O	7.00919724	10.09120544	10.49510773

O	8.84036715	9.39990091	12.23016207
N	7.69979249	11.95099334	12.38201217
S	11.60497865	14.94085746	10.12530644
S	14.77920465	12.90322796	8.79312953
S	12.54814203	14.06253708	6.20879743
S	13.51356562	10.62554002	6.30593072
S	8.42296011	12.67576117	9.31993520
S	10.83057228	11.59494259	11.88721661
S	12.08582063	8.47856550	11.55081467
S	9.77429650	9.24123497	9.15280338
S	9.68607436	11.38425141	5.84645270
S	16.07896802	13.18849588	5.34904519
Fe	12.63650843	13.63783400	8.45120408
Fe	11.75697227	12.00723657	6.71373783
Fe	9.68779755	11.23774950	8.16896613
Fe	11.51400429	10.45035796	10.01153509
Fe	13.33554448	11.15366479	8.52600265
Fe	14.32923828	12.70833797	6.61109073
Fe	10.51927552	12.84215976	10.06858705
H	12.49341660	9.68219735	8.90404109
H	13.12819305	10.93023884	10.22785559
H	12.95801522	7.78971657	10.78923153

N₂*

34

C	11.55901167	12.01574670	8.96637088
C	15.45945160	13.15385343	3.70146725
H	7.71624259	12.76232269	13.04817435
H	7.68059016	11.14033476	13.47972604
H	6.58283045	11.72396866	12.37419473
H	14.63792231	13.87156689	3.57015100
H	16.28712281	13.43434596	3.03347971
H	15.10863209	12.14799696	3.43050119
H	9.10725674	8.59436266	12.19379001
H	9.84163697	10.14584941	5.98153155
H	6.75919150	9.82535281	9.80364198
H	13.98576458	9.90346960	11.17444392
Mo	8.80264208	10.89128996	11.00042923
O	6.82841499	10.46717718	10.53296028
O	8.70349021	9.43551441	12.47481422
N	7.54121535	11.81370243	12.72207156
N	12.22642704	15.33254443	9.61860892
S	14.79735973	12.86583949	8.94464562
S	12.47268197	14.14357007	6.53818131
S	13.36405606	10.65308808	6.46789799
S	8.47119992	12.97912448	9.68467201
S	10.86831989	11.66389808	12.17177888
S	13.35758883	9.32747426	10.11586713
S	9.60176501	9.34284913	9.39491273
S	9.58089557	11.46037640	6.20823764
S	16.09244410	13.19010567	5.43117717
Fe	12.65809804	13.68286125	8.81555774
Fe	11.68771570	12.11923627	6.96783679
Fe	9.68086451	11.44131269	8.54314686
Fe	11.33764455	10.51257797	10.27925567
Fe	13.35766501	11.19304510	8.69854129

Fe	14.27829690	12.69223318	6.67648038
Fe	10.57619739	12.97222220	10.39829359
N	12.11051415	16.37086785	10.05818303

N₂H*

35

C	11.57749082	11.84441314	8.85293187
C	15.47401729	13.30938358	3.87166946
H	7.79712783	12.80456409	12.90027071
H	7.66701575	11.29003506	13.54178998
H	6.57255260	11.80960013	12.42152651
H	14.68623744	14.02221657	3.63089352
H	16.36590387	13.55364045	3.29365786
H	15.14962453	12.30118655	3.61796370
H	9.25239978	8.61708330	12.29972277
H	9.78059714	10.01690875	6.04867750
H	6.74247067	9.91523693	9.69098950
H	13.97840100	9.86735208	11.11244522
Mo	8.74986932	10.77379198	11.01996855
O	6.89763648	10.46972941	10.46493165
O	8.82516225	9.46361607	12.47499024
N	7.54842367	11.84395970	12.69846955
N	12.01120001	14.60995476	9.99569855
S	14.69412960	12.79867256	8.93085933
S	12.36036929	14.07469096	6.60567275
S	13.39438679	10.65982830	6.37525643
S	8.61637633	12.94666423	9.76578283
S	10.83844582	11.74826841	12.05687772
S	13.30489912	9.25558906	10.11598251
S	9.60191914	9.29198548	9.42506318
S	9.52786782	11.32758304	6.24076031
S	15.93539902	13.43074770	5.63716740
Fe	12.62181412	13.47401079	8.70029745
Fe	11.64310090	11.97237967	6.90146329
Fe	9.67472240	11.38609299	8.57523649
Fe	11.32141556	10.49268939	10.28266374
Fe	13.34827657	11.02566042	8.61156026
Fe	14.16109888	12.72461822	6.75597290
Fe	10.81847707	13.08447070	10.24592020
N	12.11037841	15.69335649	10.57320493
H	12.87613847	16.27266775	10.19082101

N₂H₂*

36

C	11.58301786	11.86076338	8.86089197
C	15.48479805	13.31510187	3.87456005
H	7.79375201	12.78475369	12.92856396
H	7.65698322	11.26266031	13.55650447
H	6.57176909	11.79238987	12.43222867
H	14.69207395	14.02007495	3.62715122
H	16.37204851	13.55486653	3.28885466
H	15.16381470	12.30145307	3.63690863
H	9.23906828	8.59892100	12.28352036
H	9.77017771	10.03746261	6.05500607

H	6.74516980	9.92375460	9.68577139
H	14.01154138	9.87633115	11.14828560
Mo	8.75476033	10.76554636	11.02130656
O	6.89503132	10.47589607	10.46204693
O	8.81156788	9.44151765	12.47314500
N	7.54580635	11.82605105	12.71856932
N	11.92057114	14.54899210	10.04574700
S	14.70474661	12.79878719	8.92987632
S	12.37982901	14.10265021	6.61860219
S	13.39308459	10.67681290	6.37949508
S	8.62898876	12.94668057	9.79049505
S	10.80030851	11.76371686	12.06922451
S	13.33461617	9.28518737	10.14246149
S	9.61570486	9.28990071	9.42407298
S	9.52987889	11.35202530	6.23717468
S	15.94935386	13.46105533	5.63923112
Fe	12.63209522	13.50400777	8.71716709
Fe	11.64346914	12.00477682	6.90887705
Fe	9.67253741	11.39222892	8.57281909
Fe	11.33237250	10.49713160	10.30274735
Fe	13.35118019	11.04141301	8.62498596
Fe	14.17026415	12.73715761	6.75370728
Fe	10.83942384	13.06781698	10.22831240
N	12.12574417	15.71606361	10.58382328
H	12.86710837	16.31269745	10.24313213
H	11.54094523	16.03739428	11.34236145

N*

33

C	11.56030435	11.83481584	8.85795391
C	15.49872695	13.29782533	3.84897653
H	7.77841089	12.83366879	12.89888477
H	7.68028324	11.31871998	13.54766895
H	6.58260326	11.80161128	12.41877148
H	14.71331972	14.01809190	3.61872560
H	16.38610809	13.54121910	3.26494497
H	15.16446333	12.29382590	3.59272197
H	9.24266156	8.63182393	12.33296898
H	9.80796342	9.94042589	6.09113411
H	6.74761849	9.91023054	9.72640024
H	13.99374879	9.92507660	11.13468726
Mo	8.76571175	10.78147621	11.03181272
O	6.90353189	10.46633562	10.49862855
O	8.82133000	9.48218534	12.50056654
N	7.55646244	11.86488281	12.69967593
N	11.90943439	14.47309370	9.90324817
S	14.69277644	12.85355457	8.88796955
S	12.39636285	14.03985886	6.53720363
S	13.39639625	10.65251251	6.39848962
S	8.61007651	12.92423413	9.73474496
S	10.82674163	11.77277983	12.05199160
S	13.33595548	9.30099623	10.13495010
S	9.61791183	9.26807125	9.46369428
S	9.53051472	11.24851833	6.27155001
S	15.96958165	13.41672185	5.61532970
Fe	12.61049656	13.53296045	8.66764611

Fe	11.63299180	11.95503947	6.91470241
Fe	9.68076481	11.34279461	8.59081486
Fe	11.32502214	10.49646577	10.28965075
Fe	13.34581727	11.07385931	8.63416487
Fe	14.18965949	12.71131566	6.71428076
Fe	10.80396247	13.08841927	10.22049703

NH*

34

C	11.56486306	11.82890340	8.81914672
C	15.52422365	13.35820405	3.89142946
H	7.75103452	12.83417342	12.83442344
H	7.68167608	11.33711197	13.52872800
H	6.56154876	11.77499509	12.39786332
H	14.75674074	14.09251168	3.64905370
H	16.43737437	13.60292892	3.34789737
H	15.19031148	12.36371036	3.60129619
H	9.28088560	8.66160554	12.35261647
H	9.81849577	9.82295138	6.09710181
H	6.75861294	9.84471210	9.70753368
H	13.99982397	9.89994004	11.14455152
Mo	8.75468106	10.76823004	11.00964240
O	6.90165575	10.41958656	10.46907816
O	8.84225268	9.50617089	12.50716785
N	7.53542652	11.85890802	12.66984594
N	11.82066284	14.57217327	9.82359406
S	14.69782565	12.77006563	8.88715284
S	12.35227799	13.96385704	6.43003356
S	13.43443890	10.58166448	6.38563450
S	8.57099242	12.88567598	9.68089154
S	10.80101495	11.81584822	12.02030587
S	13.31644329	9.29235963	10.15251977
S	9.63011655	9.25305615	9.46854356
S	9.55506401	11.14110469	6.22045806
S	15.93771343	13.43684837	5.67197345
Fe	12.62838115	13.52553388	8.58695725
Fe	11.64796867	11.87497510	6.85731355
Fe	9.67910372	11.31378679	8.54225994
Fe	11.32746095	10.51939453	10.28451768
Fe	13.34322952	11.01700946	8.61188271
Fe	14.15436244	12.66081392	6.71821117
Fe	10.77261117	13.09892492	10.14955997
H	11.82945422	15.55356771	10.08211338

NH₂*

35

C	11.58480216	11.85975897	8.87428481
C	15.52564065	13.33080911	3.86600209
H	7.73153107	12.75084542	12.88077017
H	7.63971606	11.24249622	13.53935466
H	6.53182902	11.72186678	12.41365115
H	14.73271648	14.06678402	3.73485344
H	16.39588223	13.64010814	3.28814840
H	15.18821646	12.35801224	3.50958655

H	9.33164904	8.60410077	12.29714763
H	9.76722152	9.85669048	6.17048945
H	6.76394748	9.90011867	9.63184644
H	13.97902476	9.77339117	11.10996769
Mo	8.73974446	10.73454716	11.01200760
O	6.89876804	10.42044652	10.43271141
O	8.83916847	9.41868325	12.45711705
N	7.50768451	11.78218751	12.68870090
N	11.90476726	14.72984149	10.01301484
S	14.77812686	12.63231390	8.88844926
S	12.37585259	13.89953643	6.42733773
S	13.36731385	10.46555172	6.41706159
S	8.57404679	12.91227926	9.76149345
S	10.79492736	11.75748413	12.06845850
S	13.25052333	9.20033732	10.12959036
S	9.63154365	9.28984067	9.42264955
S	9.55279476	11.18632854	6.27193346
S	16.03615097	13.25699949	5.62531878
Fe	12.71289400	13.51343169	8.63538143
Fe	11.66276554	11.87173700	6.89944252
Fe	9.68818407	11.38794495	8.58056315
Fe	11.32684749	10.51609503	10.29712614
Fe	13.35103368	10.97401305	8.63226955
Fe	14.21321497	12.52624664	6.65955577
Fe	10.77593917	13.08606008	10.24345414
H	11.43393989	15.56582232	9.68293416
H	12.48580778	14.99521532	10.80121241

NH₃*

36

C	11.51193176	11.85264462	8.97037841
C	15.41879942	13.30870672	3.96264939
H	7.72454283	12.59677312	12.94639251
H	7.56762759	11.03011734	13.45212841
H	6.52511454	11.63770214	12.33199082
H	14.56387598	13.94503353	3.73652198
H	16.26243160	13.60704305	3.34064317
H	15.16815723	12.27019410	3.74959748
H	9.05316193	8.40314480	12.14443922
H	9.98150488	9.81922851	6.09224377
H	6.73947338	9.60177235	9.74295943
H	13.96134656	9.74065003	11.16128271
Mo	8.72972503	10.66522067	10.96812685
O	6.86055273	10.27251396	10.42303534
O	8.68113838	9.26122702	12.37568030
N	7.48631595	11.65676384	12.65685815
N	12.63495762	15.49444488	9.68341577
S	14.70591012	12.76456667	9.08745794
S	12.26281634	14.01785971	6.55286590
S	13.43204479	10.62985100	6.49036012
S	8.41450723	12.79363733	9.64985825
S	10.75774598	11.52377086	12.18270639
S	13.30331338	9.19408275	10.11644435
S	9.62460715	9.18901590	9.39138303
S	9.64343570	11.12000013	6.21514404
S	15.92221396	13.51199534	5.71413957

Fe	12.56508309	13.54297848	8.77929735
Fe	11.65373131	11.94606695	6.98446745
Fe	9.66086052	11.28181627	8.52765227
Fe	11.31763916	10.39446239	10.31491915
Fe	13.33739072	11.06641582	8.73531292
Fe	14.16803376	12.71792390	6.83050981
Fe	10.47841040	12.77511117	10.39399244
H	11.78419611	16.03627816	9.55596469
H	12.84632051	15.48726280	10.67623608
H	13.38175741	16.01196265	9.22562777

SH-NH*

36

C	11.76710874	11.85437134	8.77462673
C	15.69564659	12.98792014	3.71055996
H	7.54806078	13.01705843	12.48570354
H	7.38414433	11.53175060	13.18561173
H	6.40260666	11.96799784	11.93317536
H	15.20244483	13.93884986	3.90588392
H	16.55501341	13.15184789	3.06093209
H	15.00020638	12.30769732	3.21995685
H	10.49137473	14.89584746	7.54581156
H	9.18959371	8.89281356	12.30106152
H	9.99780038	9.77334047	6.07604933
H	6.88656276	10.04563558	9.28760333
H	13.93926797	10.20746529	11.46985485
H	12.86142278	14.85641279	10.73364164
Mo	8.73669909	10.91922952	10.81575778
O	6.95217969	10.60783792	10.06833843
O	8.70869308	9.72700414	12.36580968
N	12.69932550	13.90686142	10.39056508
N	7.34308738	12.04113779	12.30838950
S	11.29196769	15.13559442	8.61424443
S	14.99453841	12.60305455	8.81203422
S	12.94493716	13.53894109	6.21884049
S	13.59157330	10.06451429	6.69650167
S	8.77905611	13.00452501	9.46503661
S	10.62521205	12.08562083	11.90267063
S	13.32591770	9.45006730	10.53532505
S	9.78080300	9.37195511	9.42299733
S	9.86594839	11.11498431	6.11594677
S	16.32931630	12.25990578	5.26824267
Fe	12.92075802	13.49919548	8.50449804
Fe	11.99456971	11.64445473	6.83869532
Fe	9.89429060	11.39501866	8.42356673
Fe	11.37663170	10.70995115	10.33438026
Fe	13.52359896	10.95513252	8.77933894
Fe	14.60096873	12.06088304	6.64534991
Fe	11.00623383	13.27789840	9.98114490

S-NH₂*

36

C	11.79792870	11.86350783	8.81973308
C	15.67487215	13.02276244	3.74128716

H	7.51046280	13.03876515	12.50867190
H	7.42041848	11.56245449	13.24063680
H	6.39238787	11.93658892	12.00459884
H	15.13389211	13.95172757	3.91477445
H	16.52826663	13.21891318	3.09278145
H	15.01721698	12.30040085	3.25940857
H	9.24482642	8.93632588	12.33269863
H	10.00585028	9.82240601	6.12156230
H	6.88465282	10.04240125	9.34795312
H	13.95970040	10.11327190	11.48407019
H	13.35519683	13.35359847	11.15310659
H	12.90997102	14.90326125	10.74500728
Mo	8.74184146	10.95131950	10.85265165
O	6.95676019	10.62121609	10.11625974
O	8.75614879	9.76442318	12.41206690
N	12.83340307	13.92547630	10.49544036
N	7.33756350	12.05328950	12.35575162
S	11.24595828	15.01361945	8.59594290
S	15.01323704	12.56396950	8.84460081
S	12.97221766	13.57232422	6.27938480
S	13.58760149	10.07083545	6.69971518
S	8.77912149	13.03411601	9.52122415
S	10.65022249	12.14506367	11.90687506
S	13.29610524	9.40304383	10.54714364
S	9.78773148	9.41021944	9.45998118
S	9.88173791	11.16557678	6.15365373
S	16.34100841	12.36277122	5.31588029
Fe	12.94716364	13.49520365	8.55177827
Fe	12.01303493	11.67557681	6.88056363
Fe	9.91434304	11.44523906	8.46987987
Fe	11.38880203	10.72949657	10.36770149
Fe	13.52929636	10.91915091	8.79748033
Fe	14.60513242	12.06920509	6.66472481
Fe	10.99271592	13.33555178	9.96480512

References

- [1] Mortensen, J., Hansen, L. & Jacobsen, K. Real-space grid implementation of the projector augmented wave method. *Phys. Rev. B* **71**, 035109 (2005).
- [2] Enkovaara, J. *et al.* Electronic structure calculations with GPAW: a real-space implementation of the projector augmented-wave method. *J. Phys.: Condens. Matter* **22**, 253202 (2010).
- [3] Bahn, S. R. & Jacobsen, K. W. An object-oriented scripting interface to a legacy electronic structure code. *Comput. Sci. Eng.* **4**, 56–66 (2002).
- [4] Wellendorff, J. *et al.* Density functionals for surface science: Exchange-correlation model development with Bayesian error estimation. *Phys. Rev. B* **85**, 235149 (2012).
- [5] Lee, K., Murray, É. D., Kong, L., Lundqvist, B. I. & Langreth, D. C. Higher-accuracy van der Waals density functional. *Phys. Rev. B* **82**, 081101 (2010).
- [6] Henkelman, G., Uberuaga, B. P. & Jónsson, H. A climbing image nudged elastic band method for finding saddle points and minimum energy paths. *J. Chem. Phys.* **113**, 9901 (2000).
- [7] Nørskov, J. K. *et al.* Origin of the Overpotential for Oxygen Reduction at a Fuel-Cell Cathode. *J. Phys. Chem. B* **108**, 17886–17892 (2004).
- [8] Hammer, B., Hansen, L. B. & Nørskov, J. K. Improved adsorption energetics within density-functional theory using revised Perdew-Burke-Ernzerhof functionals. *Phys. Rev. B* **59**, 7413 (1999).
- [9] Varley, J. B. & Nørskov, J. K. FirstPrinciples Calculations of Fischer–Tropsch Processes Catalyzed by Nitrogenase Enzymes. *ChemCatChem* **5**, 732–736 (2013).
- [10] Spatzal, T. *et al.* Evidence for Interstitial Carbon in Nitrogenase FeMo Cofactor. *Science* **334**, 940–940 (2011).
- [11] Lancaster, K. M. *et al.* X-ray Emission Spectroscopy Evidences a Central Carbon in the Nitrogenase Iron-Molybdenum Cofactor. *Science* **334**, 974–977 (2011).
- [12] Hoffman, B. M., Lukoyanov, D., Yang, Z.-Y., Dean, D. R. & Seefeldt, L. C. Mechanism of nitrogen fixation by nitrogenase: the next stage. *Chem. Rev.* **114**, 4041–4062 (2014).
- [13] Noodleman, L., Lovell, T., Han, W. G., Li, J. & Himmo, F. Quantum chemical studies of intermediates and reaction pathways in selected enzymes and catalytic synthetic systems. *Chem. Rev.* (2004).
- [14] Lovell, T., Li, J., Liu, T., Case, D. A. & Noodleman, L. FeMo Cofactor of Nitrogenase: A Density Functional Study of States M N, M OX, M R, and M I. *J. Am. Chem. Soc.* **123**, 12392–12410 (2001).
- [15] Kästner, J., Hemmen, S. & Blöchl, P. E. Activation and protonation of dinitrogen at the FeMo cofactor of nitrogenase. *J. Chem. Phys.* **123**, 074306 (2005).
- [16] Schimpl, J., Petrilli, H. M. & Blöchl, P. E. Nitrogen Binding to the FeMo-Cofactor of Nitrogenase. *J. Am. Chem. Soc.* **125**, 15772–15778 (2003).

- [17] Lukoyanov, D. *et al.* Testing if the Interstitial Atom, X, of the Nitrogenase Molybdenum-Iron Cofactor Is N or C: ENDOR, ESEEM, and DFT Studies of the $S=3/2$ Resting State in Multiple Environments. *Inorg. Chem.* **46**, 11437–11449 (2007).
- [18] Sandala, G. M. & Noodleman, L. Modeling the MoFe Nitrogenase System with Broken Symmetry Density Functional Theory. In *Nitrogen fixation : methods and protocols*, 293–312 (Humana Press, Totowa, NJ, 2011).
- [19] Harris, T. V. & Szilagy, R. K. Comparative Assessment of the Composition and Charge State of Nitrogenase FeMo-Cofactor. *Inorg. Chem.* **50**, 4811–4824 (2011).
- [20] Bjornsson, R., Neese, F., Schrock, R. R. & Einsle, O. The discovery of Mo (III) in FeMoco: reuniting enzyme and model chemistry. *JBIC Journal of ...* (2015).
- [21] Spatzal, T., Perez, K. A., Einsle, O., Howard, J. B. & Rees, D. C. Ligand binding to the FeMo-cofactor: Structures of CO-bound and reactivated nitrogenase. *Science* **345**, 1620–1623 (2014).
- [22] Cramer, S. P., Hodgson, K. O., Gillum, W. O. & Mortenson, L. E. The molybdenum site of nitrogenase. Preliminary structural evidence from x-ray absorption spectroscopy. *J. Am. Chem. Soc.* **100**, 3398–3407 (1978).
- [23] Huang, H. Q., Kofford, M., Simpson, F. B. & Watt, G. D. Purification, composition, charge, and molecular weight of the FeMo cofactor from *azotobacter vinelandii* nitrogenase. *Journal of Inorganic Biochemistry* **52**, 59–75 (1993).
- [24] Hinnemann, B. & Nørskov, J. K. Catalysis by Enzymes: The Biological Ammonia Synthesis. *Top Catal* **37**, 55–70 (2006).
- [25] Dance, I. The hydrogen chemistry of the FeMo-co active site of nitrogenase. *J. Am. Chem. Soc.* **127**, 10925–10942 (2005).
- [26] Peterson, A. A., Abild-Pedersen, F., Studt, F., Rossmeisl, J. & Nørskov, J. K. How copper catalyzes the electroreduction of carbon dioxide into hydrocarbon fuels. *Energy Environ. Sci.* **3**, 1311 (2010).
- [27] Varley, J. B. *et al.* Ni–Fe–S Cubanes in CO₂ Reduction Electrocatalysis: A DFT Study. *ACS Catal.* **3**, 2640–2643 (2013).
- [28] Karlberg, G. S. & Wahnström, G. Density-functional based modeling of the intermediate in the water production reaction on Pt (111). *Phys. Rev. Lett.* **92**, 136103 (2004).
- [29] Tripkovic, V., Skúlason, E., Siahrostami, S., Nørskov, J. K. & Rossmeisl, J. The oxygen reduction reaction mechanism on Pt(111) from density functional theory calculations. *Electrochimica Acta* **55**, 7975–7981 (2010).
- [30] Studt, F., Abild-Pedersen, F., Varley, J. B. & Nørskov, J. K. CO and CO₂ hydrogenation to methanol calculated using the BEEF-vdW functional. *Catal. Lett.* **143**, 71–73 (2013).
- [31] Hinnemann, B. *et al.* Biomimetic Hydrogen Evolution: MoS₂ Nanoparticles as Catalyst for Hydrogen Evolution. *J. Am. Chem. Soc.* **127**, 5308–5309 (2005).

- [32] Hansen, H. A., Varley, J. B., Peterson, A. A. & Nørskov, J. K. Understanding Trends in the Electrocatalytic Activity of Metals and Enzymes for CO₂ Reduction to CO. *J. Phys. Chem. Lett.* **4**, 388–392 (2013).
- [33] Shi, C., O’Grady, C. P., Peterson, A. A., Hansen, H. A. & Nørskov, J. K. Modeling CO₂ reduction on Pt(111). *Phys. Chem. Chem. Phys.* **15**, 7114–7122 (2013).
- [34] Seefeldt, L. C., Hoffman, B. M. & Dean, D. R. Mechanism of Mo-Dependent Nitrogenase. *Annu. Rev. Biochem.* **78**, 701–722 (2009).
- [35] Hageman, R. V. & Burris, R. H. Nitrogenase and Nitrogenase Reductase Associate and Dissociate with Each Catalytic Cycle. *Proceedings of the National Academy of Sciences of the United States of America* **75**, 2699–2702 (1978).
- [36] Kästner, J. & Blöchl, P. E. Ammonia Production at the FeMo Cofactor of Nitrogenase: Results from Density Functional Theory. *J. Am. Chem. Soc.* **129**, 2998–3006 (2007).
- [37] Medford, A. J. *et al.* Assessing the reliability of calculated catalytic ammonia synthesis rates. *Science* **345**, 197–200 (2014).
- [38] Chase, W., Society, A. C., American Institute of Physics, National Institute of Standards & Technology. *NIST-JANAF Thermochemical Tables*. Journal of physical and chemical reference data: Monograph (American Chemical Society, 1998).
- [39] *CRC Handbook of Chemistry and Physics* (<http://www.hbcpnetbase.com>).
- [40] *The Landolt-Bornstein Database. Thermodynamic Properties of Compounds* (<http://materials.springer.com>).
- [41] Giannozzi, P. *et al.* QUANTUM ESPRESSO: a modular and open-source software project for quantum simulations of materials. *J. Phys.: Condens. Matter* **21**, 395502 (2009).
- [42] Burgess, B. K. & Lowe, D. J. Mechanism of molybdenum nitrogenase. *Chem. Rev.* **96**, 2983–3012 (1996).
- [43] Seefeldt, L. C., Hoffman, B. M. & Dean, D. R. Electron transfer in nitrogenase catalysis. *Curr. Opin. Chem. Biol.* **16**, 19–25 (2012).
- [44] Pickett, C. J. *et al.* ElectronTransfer Chemistry of the Iron–Molybdenum Cofactor of Nitrogenase: Delocalized and Localized Reduced States of FeMoco which Allow Binding of Carbon Monoxide to Iron and Molybdenum. *Chem. Eur. J.* **9**, 76–87 (2003).
- [45] Davis, L. C., Henzl, M. T., Burris, R. H. & Orme-Johnson, W. H. Iron-sulfur clusters in the molybdenum-iron protein component of nitrogenase. Electron paramagnetic resonance of the carbon monoxide inhibited state. *Biochemistry* **18**, 4860–4869 (1979).
- [46] Hu, Y., Lee, C. C. & Ribbe, M. W. Extending the Carbon Chain: Hydrocarbon Formation Catalyzed by Vanadium/Molybdenum Nitrogenases. *Science* **333**, 753–755 (2011).
- [47] Yang, Z.-Y., Dean, D. R. & Seefeldt, L. C. Molybdenum nitrogenase catalyzes the reduction and coupling of CO to form hydrocarbons. *Journal of Biological Chemistry* **286**, 19417–19421 (2011).